 doi:10.20944/preprints202007.0626.v1

Influence of substrate, process conditions, and post-annealing temperature on the properties of ZnO thin films grown by SILAR method

Bijoy Chandra Ghos[1†, 2], Md. Alauddin Hossain[2], Nazmul Islam Tanvir[1], Shanta Majumder[1†, 2], Mohammad Atiqur Rahman[2, *], Md Abdul Majed Patwary[2,3,*] and Syed Farid Uddin Farhad[1,*]

[1] Energy Conversion and Storage Research Section, Industrial Physics Division, BCSIR Labs, Dhaka 1205, Bangladesh Council of Scientific and Industrial Research (BCSIR), Bangladesh; nazmul.tanvir88@gmail.com (N.I.T.)

[2] Physical Chemistry Research Laboratory, Department of Chemistry, Comilla University, Cumilla 3506, Bangladesh; bijoycou037@gmail.com (B.C.G.), alauddincou21@gmail.com (M.A.H.), shantamajumder4@gmail.com (S.M.)

[3] Department of Electrical and Electronic Engineering, Saga University, Honjo, Saga 840-8502, Japan

[†] Student during postgraduates research in ECSR, IPD.

* Correspondence: sf1878@my.bristol.ac.uk (S.F.U. Farhad), mamjedp@gmail.com (M.A.M. Patwary), atiqche31@yahoo.com (M.A. Rahman).

Abstract: Here we report the effect of substrate, sonication process, and post-annealing on the structural, morphological, and optical properties of ZnO thin films grown in presence of isopropyl alcohol (IPA) at temperature 30 – 65 ℃ by SILAR method on both soda lime glass (SLG) and Cu foil. The X-ray diffraction (XRD) patterns confirmed the preferential growth of ZnO thin films along (002) and (101) plane while grown on SLG and Cu foil substrate respectively. Both XRD and Raman spectra confirmed the ZnO and Cu-oxide phases of the deposited films. Scanning electron microscope (SEM) image of the deposited films shows compact and uniformly distributed grains for

 doi:10.20944/preprints202007.0626.v1

samples grown without sonication while using IPA at temperature 50 and 65 ℃. The post-annealing treatment improves the crystallinity of the films, further evident by XRD and UV-VIS-NIR results. The estimated optical bandgaps are in the range of 3.37-3.48 eV for as-made samples. Results revealed that high-quality ZnO thin films could be grown without sonication using IPA dispersant at 50 ℃, which is much lower than the reported results using the SILAR method. This study suggests that in the presence of IPA, the SLG substrate results in better c-axis oriented ZnO thin films than that of DI water, ethylene glycol, propylene glycol at the optimum temperature of 50 ℃. Air-annealing of the samples grown on Cu foils induced the formation of CuxO/ZnO junctions which is evident from the characteristic I-V curve including the structural and optical data.

Keywords: ZnO thin films, SILAR, IPA dispersant, copper oxide, Post-annealing, c-axis orientation

---

1. Introduction

ZnO is amongst the most widely used n-type metal oxide semiconductor materials because of its unique structural, optical and electrical properties in conjugation with cheap, non-toxic nature, and natural abundance [1-3]. It has distinctive optoelectronic and physical properties such as tunable direct wide bandgap of about 3.37 eV, high transparency (>80 %) in the visible region, and large exciton binding energy (60 meV) at room temperature [4-12], optimum refractive index (n ≈ 2.0), notable electron mobility (as large as 155 $cm^2/V.s$) [13,14,15]. Moreover, ZnO are chemically and thermodynamically stable and basically crystallizes in the hexagonal wurtzite structure [16].

 doi:10.20944/preprints202007.0626.v1

All the above unique features make ZnO a suitable material for diverse applications including anti-reflective coating (ARC), solar cells, and transparent conductive oxide for flat panel displays [17,18], photodiodes [19], gas sensors [20,21], light emitting diodes [22], surface acoustic waves [23], protective surface coatings [24], piezoelectric transducers [25] etc. These potential applications have boosted research related to the development of better quality ZnO thin films over the span of ongoing decades.

Both physical and chemical methods have been used for the synthesis of ZnO thin films for instances, successive ionic layer adsorption and reaction (SILAR) [26,27], chemical bath deposition (CBD) [28], pulsed laser deposition (PLD) [29], RF magnetron sputtering [30], metal organic chemical vapour deposition (MOCVD) [31], sol-gel derived dip coating [32], spray pyrolysis [16], hydrothermal [33], molecular beam epitaxy [34], drop casting [35], and different sol-gel derived spin coating [36] techniques etc. Among them, SILAR is one of the simplest and economically favorable chemical methods because it produces durable and adherent thin films comparatively at low processing temperatures and does not need any sophisticated and modern instruments [36,37]. Furthermore, this technique consents bulk region deposition on various substrates as soda lime glass (SLG) microscopy slides, fluorine doped tin oxides (FTO), and Cu foil substrates etc. [16,38,39]. The deposition technique relies on bath temperature, solution pH, complexing and dispersant agents and rinsing procedures [40-44] etc.

To our best knowledge, only a few reports have been published so far regarding the deposition of ZnO thin films using Cu foil. Raidou et al. [45] have grown ZnO thin films on three kinds of substrates such as Cu, Si, and glass by the SILAR method. They have showed that the structure of the film depends strongly on the nature of the substrate for instance, ZnO particles deposited on Cu

Preprints (www.preprints.org) | NOT PEER-REVIEWED | Posted: 26 July 2020 doi:10.20944/preprints202007.0626.v1

substrate formed hexagonal structure whereas spindles shape was formed on the Si substrate and for glass substrate the film was in the form of small flowers and prisms.

Gao et al. [27] first reported ZnO thin films deposition by incorporating an ultrasonic rinsing step in the SILAR method. Subsequently, Shei et al. improved the process and investigated the effects of deionized water (DI), ethylene glycol, and propylene glycol between the rinsing steps as well as rinsing temperature on the structural and optical properties of ZnO thin films. In those cases, ethylene glycol imposes environmental risks [5]. They reported that higher growth temperature is necessary to produce highly c-axis oriented ZnO thin films when using ethylene glycol and propylene glycol during the rinsing processes [5,46,47]. To address above issues, this study aims to investigate the influence of sonication, usage of isopropyl alcohol (IPA) dispersant, and thereafter post-annealing effect on the structural, morphological and optical properties of SILAR deposited ZnO thin films on SLG and Cu foil substrates. Cu foils were chosen mainly to investigate the copper oxide forming conditions near the ZnO nucleation cite, as well as the formation of Cu_2O/ZnO or CuO/ZnO junctions depending on IPA and post-annealing temperature. The use of IPA has pronounced effect as dispersing agent over others and the post-annealing is beneficial for making Cu_xO/ZnO (x = 1 or 2) heterojunction. The experimental results are presented and discussed below.

2. Materials and Methods

2.1. Materials

In this work, zinc chloride ($ZnCl_2$, purity~ 98 %, Scharlau), isopropyl alcohol ($(CH_3)_2CHOH$; purity ~99.70 %, Active Fine Chemicals) and concentrated ammonia (NH_4OH, ~28% solution, Merck Millipore) were used. All the reagents were of analytical grade and used without further purification.

Preprints (www.preprints.org) | NOT PEER-REVIEWED | Posted: 26 July 2020 doi:10.20944/preprints202007.0626.v1

Both non-conducting SLG (40×25×1 mm^3) and conducting thin Cu foil (40×20×0.2 mm^3) were used to deposit ZnO thin films.

2.2. Synthesis of ZnO Thin Films

ZnO thin films were deposited simultaneously both on SLG and Cu foil substrates by using a similar SILAR method describe elsewhere [41]. Briefly, the SLG were cleaned with detergent followed by successive cleaning in an ultrasonic bath using DI water, toluene, acetone, isopropyl alcohol and again DI water each for 15 minutes. On the other hand, Cu foils were treated with cottonwood soaked in 10M HNO_3 solution and finally dried in air. Prior to the film deposition, zinc complex ($[Zn(NH_3)_4]^{2+}$) precursor solution was prepared by mixing 0.1 M $ZnCl_2$ and concentrated (~28 %) ammonia solution (NH_4OH). NH_4OH was added to adjust the solution pH 10 [46,47]. Subsequently, both SLG and Cu foil (tied back to back) [41] were immersed together into the precursor zinc-complex solution and then dipped into unheated deionized water each for 20 seconds which results in the formation of $Zn(OH)_2$ precipitate.

Additionally, counter ion (Cl^-) and coarsely adhered $Zn(OH)_2$ grains were removed from the substrate by immersing it into ultrasonic-assisted DI water for 30 seconds. Furthermore, the substrates were treated with IPA for 20 seconds to form ZnO. IPA acted as a dispersing agent which reduced the ZnO agglomeration and enhance the decomposition capability of $Zn(OH)_2$ to ZnO when the temperature was increased from room temperature (~30 ℃) to 65 ℃. Finally, the substrates were dipped into ultrasonic-assisted DI water (see Figure 1). Likewise, the above steps were repeated up to 20 times for preparing the sample with IPA at 30, 50 and 65 ℃ labeled the as-deposited samples as IPA30, IPA50, and IPA65. The same deposition procedure was repeated by

Preprints (www.preprints.org) | NOT PEER-REVIEWED | Posted: 26 July 2020 doi:10.20944/preprints202007.0626.v1

eliminating the sonication step. The most important deposition parameters and processing conditions are summarized in Table 1.

Table 1. Sampling details for the deposition of ZnO thin films with IPA at different temperature.

Deposition temperature (^{0}C)	Glass substrate		Copper foil substrate	
	Sonication	*Without sonication*	*Sonication*	*Without sonication*
30	G1	G4	C1	C4
50	G2	G5	C2	C5
65	G3	G6	C3	C6

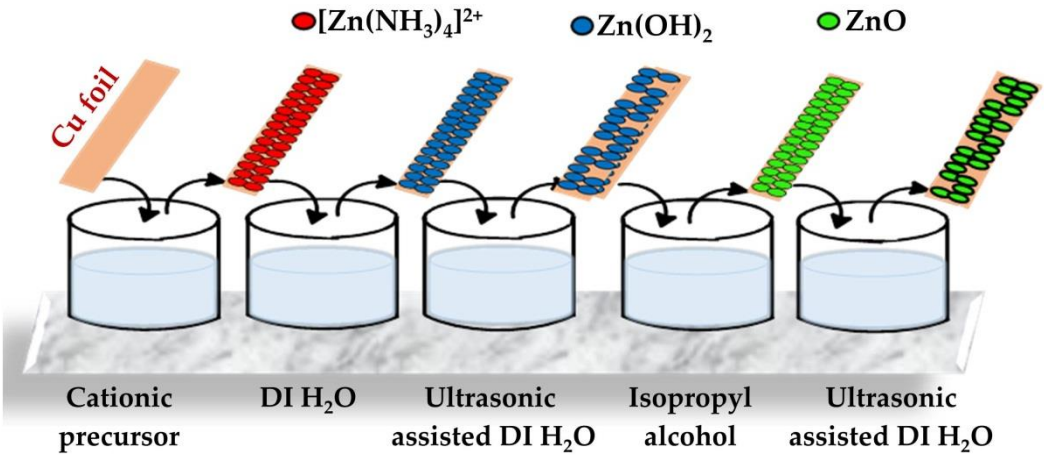

Figure 1. Schematic diagram showing the deposition of ZnO thin film on Cu foil using IPA at different temperature.

The overall reactions involved in the ZnO film deposition are given below [5]:

$$[Zn(NH_3)_4]^{2+} + 4H_2O \longrightarrow Zn^{2+} + 4NH_4^{+} + 4OH^{-}$$

$$Zn^{2+} + 2OH^{-} \longrightarrow Zn(OH)_2(s)$$

$$Zn(OH)_2(s) \longrightarrow ZnO(s) + H_2O$$

After deposition, the samples were thoroughly rinsed by DI water, and then dried under laboratory atmosphere and safely stored into the sample boxes for characterization. Some of the samples were

Preprints (www.preprints.org) | NOT PEER-REVIEWED | Posted: 26 July 2020 doi:10.20944/preprints202007.0626.v1

cut into equal pieces for subsequent characterizations as well as 1 hour air-annealing at 250 ℃; while one piece of each batch were kept as as-deposited sample for reference.

2.3. Characterization techniques

The structural properties and phase of the deposited thin films were characterized by XRD (Philips PANalytical X'Pert MRD) with a CuKα (λ = 0.15406 nm) radiation source in θ-2θ coupled mode and Raman spectroscopy (Horiba HR800) with 488 nm laser excitation (P≤ 5 mW). Surface morphologies of the samples were imaged by scanning electron microscope (SEM) (Philips XL30 EEG SEM).The optical properties were examined by using a double-beam UV-Visible-NIR spectrophotometer (Shimadzu UV 2600 ISR plus) in the range of 220-1400 nm. Both diffuse reflection and transmission spectra were taken to eliminate substrate contributions [35] where necessary.

3. Results and Discussion

3.1. Structural Characterization

The phase and crystal structure of both as-deposited and annealed samples were examined by XRD ranging from 2θ = 25-45° and the relating XRD patterns are shown in Figure 2. The deposited samples grown on SLG exhibited three intense peaks at 2θ ≈31.74°, 34.40° and 36.21° which corresponds respectively to (100), (002) and (101) planes of ZnO hexagonal wurtzite structure [35]. No diffraction peaks of $Zn(OH)_2$ are discernible in the XRD patterns (see Figure 2a). In the case of samples deposited on Cu foil, thin films are preferably deposited along the (101) plane of ZnO, where the diffraction peak at 2θ ≈ 43.5° corresponds to the Cu (111) plane arising from the

Preprints (www.preprints.org) | NOT PEER-REVIEWED | Posted: 26 July 2020 doi:10.20944/preprints202007.0626.v1

underlying substrate (see Figure 2b). All of the Cu foil samples produced Cu_xO/ZnO (x = 1, 2) structure after post-annealing at 250 ℃ irrespective of the growth temperature with IPA and sonication process (see top panels in Figure 2). This may be due to the oxidation of Cu foil substrate as can be seen from both XRD and Raman spectra depicted in Figure 2b and Figure 3b. These results suggest the formation of Cu-oxide/ZnO heterojunction depend only on the post-annealing but not on the sonication process and IPA dispersant. Thus, the post-annealing is beneficial for the formation of Cu_xO/ZnO heterojunctions [16,45,48]. It is evident from the Figure 2a, the strong preferential growth along (002) plane of ZnO observed for samples grown on SLG suggesting highly c-axis oriented films [35] while preferred orientation along (101) plane for samples deposited on Cu foil [45] as can be seen in Figure 2b. Thus, the crystal growth is strongly influenced by the substrate types. The strong peak along (002) plane for the as-deposited G5(IPA50) and G6(IPA65) samples signifies highly oriented c-axis ZnO films [35] which is absent for G4(IPA30) samples, suggesting that temperature of IPA promotes crystallinity of the as-deposited ZnO film. The intensity of the concerned diffraction peak is seen to increase further after post-annealing. Therefore, increasing the IPA temperature and post-annealing improved the crystallinity of the deposited thin films [35,46]. The same trend is observed for samples deposited on Cu foil. In both cases, without sonication, samples exhibited better crystallinity as shown in Figure 2 and the good quality films formed using IPA with a minimum of 50 ℃. Shei *et al.* [5,46] have reported no film growth below 75 and 95 ℃ respectively by using ethylene glycol and propylene glycol.

Preprints (www.preprints.org) | NOT PEER-REVIEWED | Posted: 26 July 2020 doi:10.20944/preprints202007.0626.v1

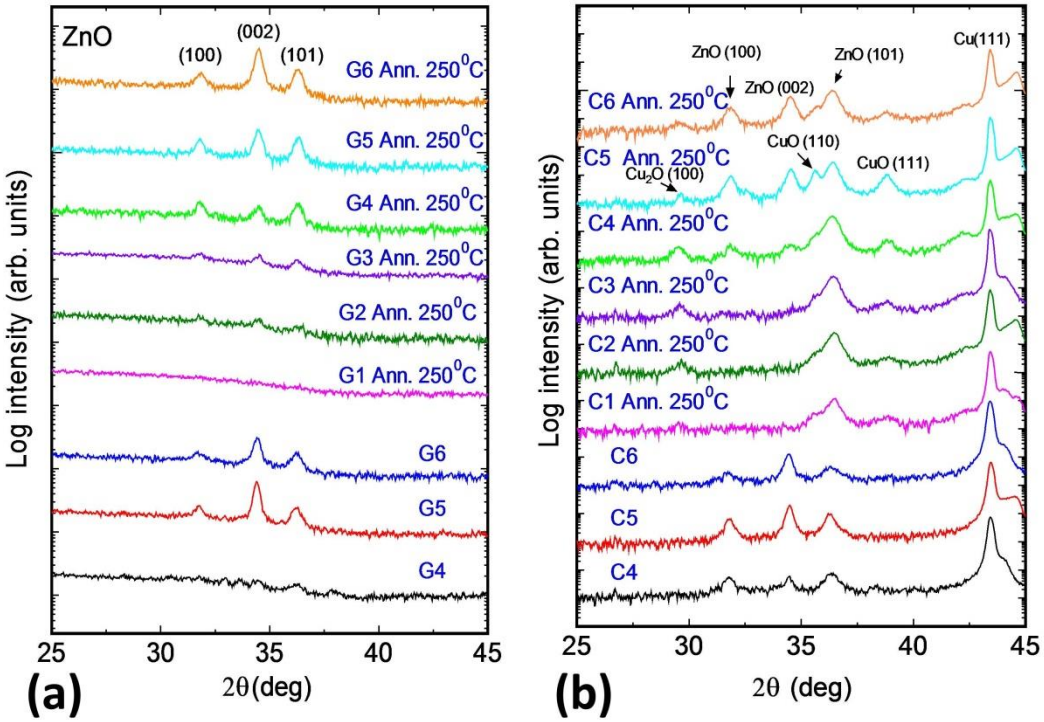

Figure 2. XRD patterns of both as-made and post-annealed samples grown on **(a)** SLG and **(b)** Cu foil. The diffraction peaks of corresponding materials are shown by arrow sign for clarity.

It is also evident from Figure 2a that highly textured films can be prepared for samples G5(IPA50) and G6(IPA65) without sonication steps. This may be due to the fact that IPA acts as a better dispersant compared to ethylene glycol, propylene glycol and DI water reported in refs. [5,46,47] and results in depositing better quality ZnO thin films.

The important structural parameters and mean crystallite sizes (D) of SLG-samples were calculated by using Scherrer equation [49] to the 002 diffraction peak of ZnO and summarized in Table 2:

$$D = \frac{k\lambda}{\beta cos\theta} \quad (1)$$

Where, λ= Wavelength of X-ray (0.15406 nm for CuKα radiation source), k= constant which is 0.94, β = Full width at half maxima (FWHM), θ= Diffracted angle (FWHM and 2θ are in degrees).

Preprints (www.preprints.org) | NOT PEER-REVIEWED | Posted: 26 July 2020 doi:10.20944/preprints202007.0626.v1

Table 2. Mean crystallite size and lattice strain of as-made and annealed samples deposited on SLG using IPA at different temperatures.

Sample	2θ (deg.)	FWHM (deg.)	Crystallite size (nm)	Lattice strain (ε) × 10^{-3}
G4(IPA30)	34.37	0.73	12	10.3
G4 Ann. 250 ℃	34.51	0.63	14	8.9
G5(IPA50)	34.41	0.37	23	5.2
G5 Ann. 250 ℃	34.48	0.45	19	6.3
G6(IPA65)	34.48	0.48	18	6.7
G6 Ann. 250 ℃	34.51	0.41	21	5.8

It is evident from the Table 2 that the mean crystallite sizes were 12-23 nm and 18-21 nm respectively for as-deposited and annealed samples grown on SLG. The crystallite size shows an increasing trend and the lattice strain decreases with post-annealing at 250 ℃ (G4 Ann. 250 ℃ and G6 Ann.250 ℃) which signifies the improvement of the crystallinity [5] of the films as can be seen from Figure 2a. The sample deposited on SLG at 50 ℃ (G5) in the absence of sonication exhibited the highest crystallinity (D = 23 nm) and minimum lattice strain among all samples with (002) preferential growth. Therefore, these observations indicated the optimum temperature in presence of IPA should be 50 ℃ for growing better quality c-axis oriented ZnO thin films without sonication steps.

3.2. Raman Analysis

Room temperature Raman measurements of samples deposited on both SLG and Cu foil were carried out to identify the phase purity of Zn- and Cu-oxides as well as to investigate the effect of processing conditions on their crystalline structure. Raman spectroscopy is an effective tool to analyze the small changes as the vibrational signals are very sensitive to the local environment of

Preprints (www.preprints.org) | NOT PEER-REVIEWED | Posted: 26 July 2020 doi:10.20944/preprints202007.0626.v1

the molecule, crystal structure, chemical bond, etc. [50]. The Raman spectra of the samples deposited on both SLG and Cu foil are shown in Figure 3a and Figure 3b respectively.

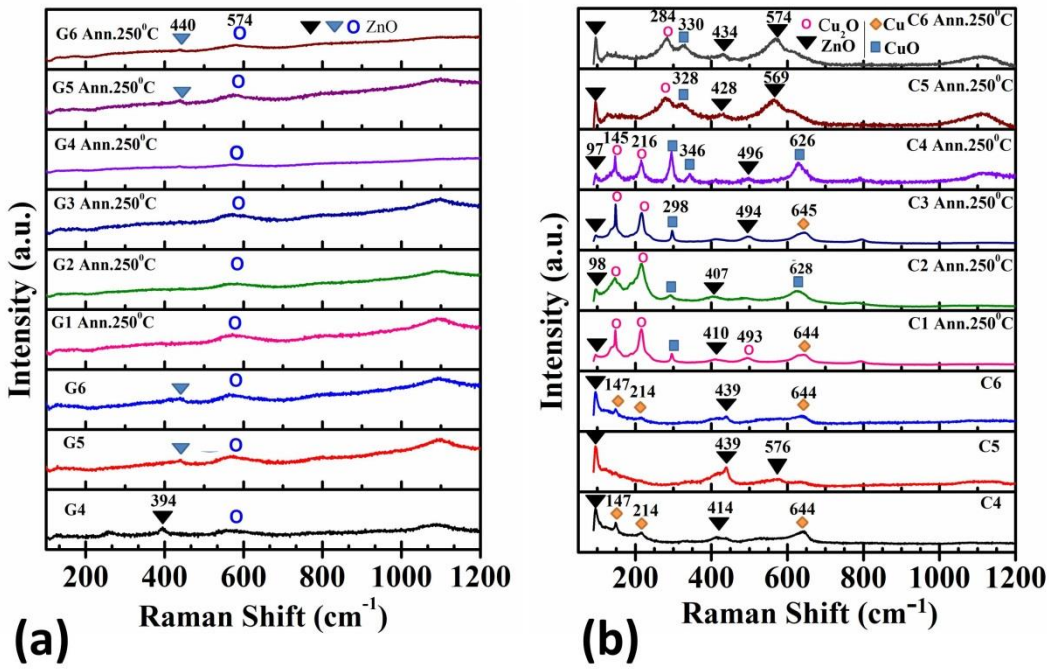

Figure 3. Raman spectra of the samples grown on **(a)** SLG and **(b)** Cu foil. The reference Raman shift values are indicated by different symbols in the figure.

It is clear from Figure 3a that the post-annealing exhibited a broad Raman signal approximately at 574 cm^{-1} which could be attributed to ZnO [51] for samples G1 Ann 250 ℃ and G2 Ann.250 ℃ for which XRD peaks were not clear in Figure 2a. In contrast, the samples G5(IPA50) and G6(IPA65) (without sonication) showed two distinguishable peaks centering at ~440 and ~574 cm^{-1} which have been attributed to highly crystalline c-axis oriented ZnO films due to a decrease of defects in the interior of the crystal [51].

In Figure 3b, the films on Cu foil show Raman peaks centering at 97, 98, 405, 407, 410, 428, 434, 494, 496, 569 and 574 cm^{-1} correspond to ZnO phase. Moreover, the Raman signals for copper oxide (Cu_2O + CuO) mixture phases were evidenced for all annealed samples (C1 Ann. 250 ℃ to C6 Ann.

Preprints (www.preprints.org) | NOT PEER-REVIEWED | Posted: 26 July 2020 doi:10.20944/preprints202007.0626.v1

250 ℃). In addition, peaks at around 147, 214, 644 cm^{-1} appeared for samples grown on the Cu foil. The new Raman shift appeared close to 145, 216, 284, 493 cm^{-1} confirmed the existence of Cu_2O phase while those close to 298, 330, 346, 626 cm^{-1} are attributed to CuO phase [50-59]. These observations are indicating the possibility of the facile Cu_xO/ZnO formation by post-annealing at temperature as low as 250 ℃. These results are also in consistent with the observed XRD pattern shown in Figure 2b. From both XRD and Raman analyses, it can be concluded that for depositing phase pure highly crystalline c-axis oriented ZnO films, it may be better to deposit on SLG and post-annealing at 250 ℃ for 1 hour results the formation of Cu-oxide/ZnO heterojunction for films grown on Cu foil.

3.3. Morphological characterization

Figure 4 compares the surface morphologies of thin films grown on both SLG and Cu foil. From Figure 4a and 4d, it is clearly seen that the samples deposited using IPA at 30 ℃ exhibits cotton-like amorphous morphology (see also XRD patterns in figure 2). In contrast, compact and uniformly distributed spherical grains were observed both for IPA50 and IPA65 as-deposited samples. Thus, at relatively high temperatures good quality films are produced as it provides sufficient energy for complete conversion of $Zn(OH)_2$ to ZnO [5]. The grain sizes of the films grown on SLG were larger (~260-300 nm) compared to those grown on Cu foil (~200-230 nm) further indicating better quality films which supports the XRD data. Some overgrown clusters for Cu foil-samples can be seen which might be detrimental for device applications. Thus, the film growth quality is not only affected by the temperature of the IPA but also the types of substrate. Previous studies reported that relatively higher temperature (≥ 95 ℃) was required to decrease agglomeration for ethylene glycol and propylene glycol used as dispersing agent [5,46]. Since

Preprints (www.preprints.org) | NOT PEER-REVIEWED | Posted: 26 July 2020 doi:10.20944/preprints202007.0626.v1

isopropyl alcohol is a monohydric alcohol, it forms only inter-molecular hydrogen bond [60] and affects the deposition process free from releasing thermal energy due to the breaking of intra-molecular H-bonding. Consequently, $Zn(OH)_2$ species are easily removed through H-bonding which are loosely adsorbed on the ZnO surface. This property makes IPA to act as a better dsipersant than ethylene glycol and propylene glycol at relatively low temperatures [61]. The IPA50 sample grown without sonication exhibited a compact microstructural morphology together with appreciable crystallite size (D = 23 nm) and optical band gap (Eg = 3.37 eV). These observations assert that the surface morphologies can be controlled by controlling the IPA temperature and by selecting a suitable substrate.

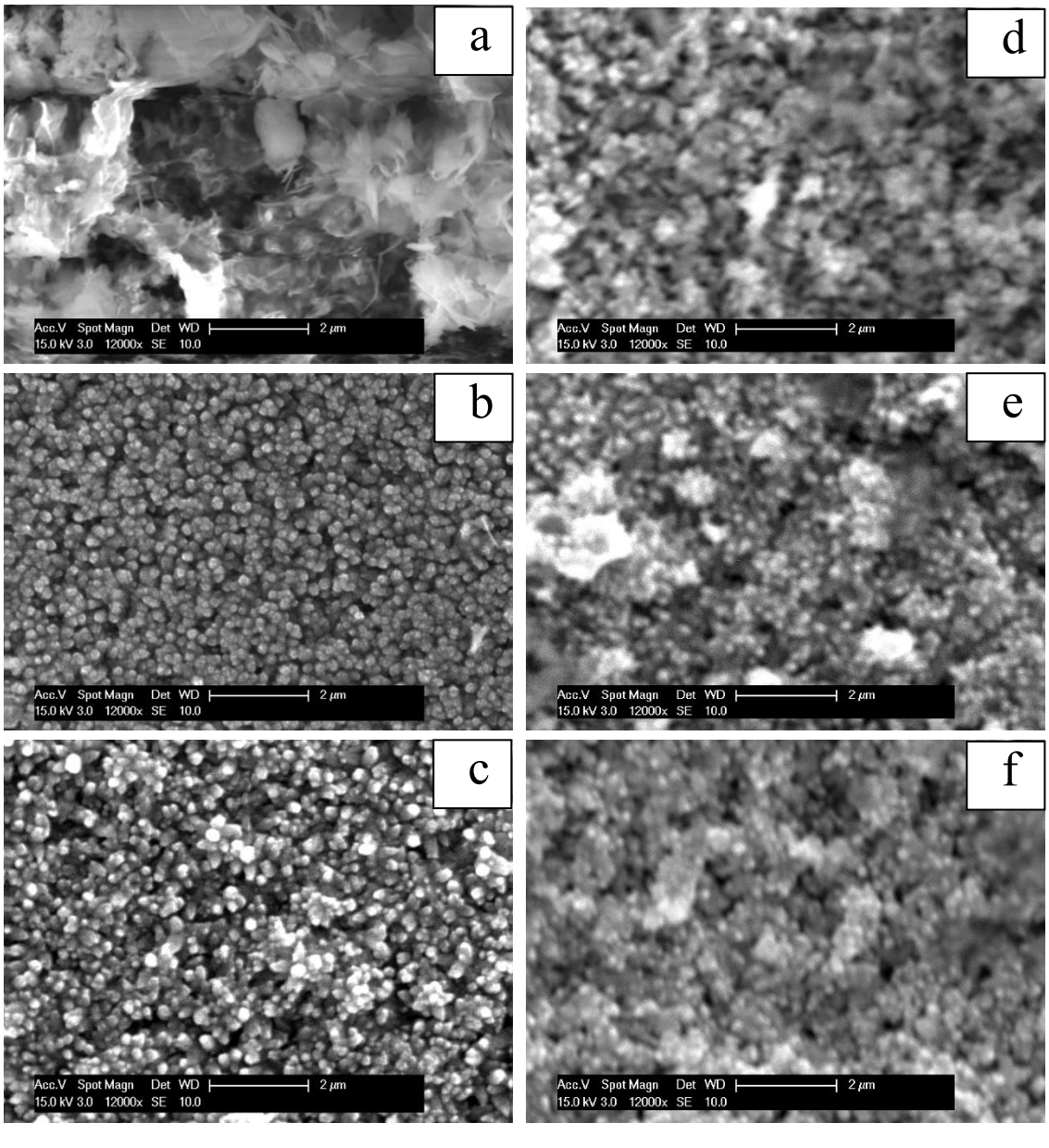

Preprints (www.preprints.org) | NOT PEER-REVIEWED | Posted: 26 July 2020 doi:10.20944/preprints202007.0626.v1

Figure 4. SEM micrographs of the samples deposited using IPA dispersant at various temperatures on SLG **(a)** G4(30 ℃), **(b)** G5(50 ℃),, **(c)** G6(65 ℃),; and on Cu foil **(d)** C4(30 ℃),, **(e)** C5(50 ℃),, **(f)** C6(65 ℃),

3.4. Optical characterization

To elucidate the optical characteristics of the as-grown and annealed samples on SLG, both transmission and diffuse reflection spectra were taken for eliminating underlying substrate contribution [35]. In case of the samples deposited on Cu foil, only the reflection spectra were recorded. The diffuse reflection spectra of samples grown without the sonication process at different temperatures with IPA have been included in Figure 5.

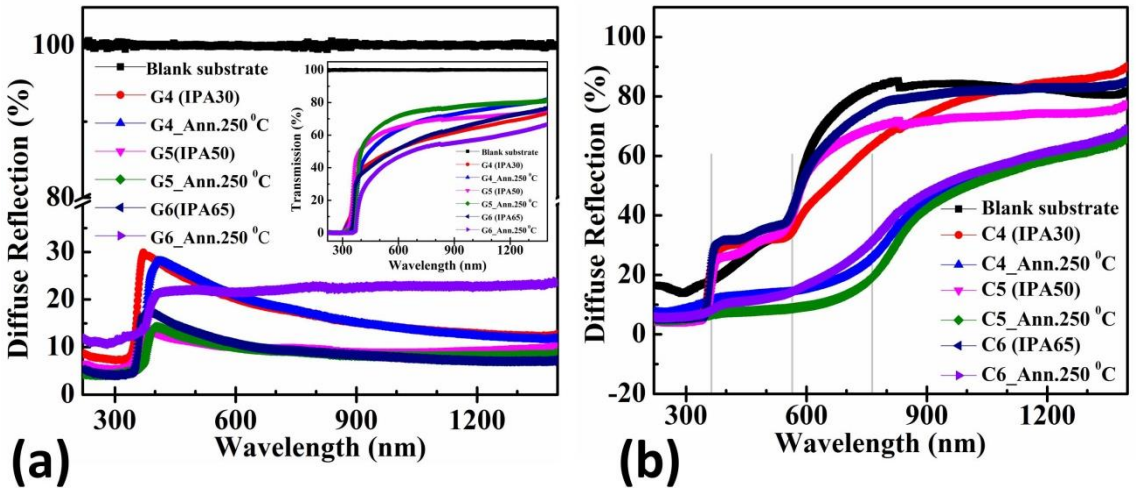

Figure 5. Diffuse reflection spectra of the samples deposited on **(a)** SLG **(b)** Cu foil. Both as-deposited and annealed samples have been included in the same graph. The corresponding transmission spectra of samples grown on SLG also inserted into Figure 5a for comparison purposes. The vertical lines in Figure 5b indicating the approximate absorption edge of ZnO, Cu_2O and CuO.

From Figure 5a it is clearly seen that the samples grown on SLG shows 10-20% reflection in the visible region and transparency of 75~80% (figure 5a inset). A sharp absorption edge near

Preprints (www.preprints.org) | NOT PEER-REVIEWED | Posted: 26 July 2020 doi:10.20944/preprints202007.0626.v1

wavelength, $\lambda \approx 380$ nm can be seen from both transmission and reflection data which corresponds to ZnO thin films [35]. Samples grown with IPA at higher temperatures (50 and 65 ℃) exhibit enhanced transparency which further confirmed the better crystallinity and film growth with fewer defects in the interior crystal [5] and supports the XRD data. In contrast, for the samples grown on Cu foil (Figure 5b); sharp absorption edges near $\lambda \approx$380, 580 and 780 nm can be clearly seen (see fade verticle lines) which could be attribute to ZnO, Cu_2O and CuO phase respectively [41,50,62]. The presence of mixed (Cu_2O + CuO) phases formed on Cu foil were also confirmed from the XRD and Raman spectra shown in Figure 2b and Figure 3b.

The optical bandgap was estimated from the Tauc plot generated by using the reflection data and the Kubelka-Munk function ($F(R_\infty)$ [35] represented by equation:

$$(h\upsilon F(R_\infty))^n = A(h\upsilon - E_g) \quad (2)$$

Where, E_g= Bandgap energy, R_∞= Diffuse reflection, h = Planck's constant and υ = Frequency of the incident light. ZnO is a direct bandgap material (n=2) which showed direct forbidden transition at wavelength $\lambda \approx$380 nm. Therefore, putting n = 2 in the above equation, the E_g values obtained by plotting $(h\upsilon F(R_\infty))^2$ vs $h\upsilon$, where the quantity $(h\upsilon F(R_\infty))^2$ extrapolated to zero [35,41]. The bandgap plots are shown in Figure 6 and E_g values together with XRD and Raman data are listed in Table 3.

Preprints (www.preprints.org) | NOT PEER-REVIEWED | Posted: 26 July 2020 doi:10.20944/preprints202007.0626.v1

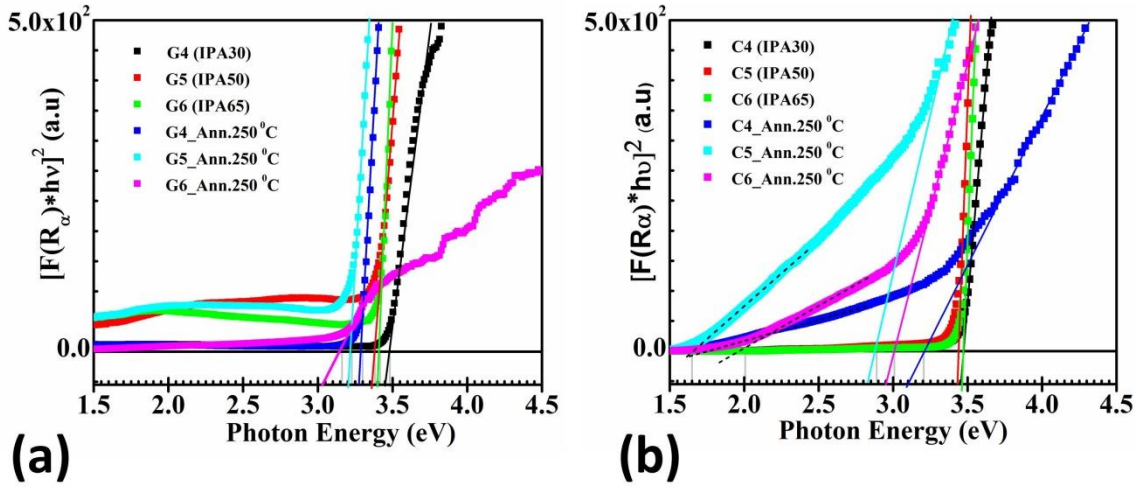

Figure 6. Tauc plots of the samples grown on **(a)** SLG **(b)** Cu foil using diffuse reflection data. The E_g values are calculated by extrapolating the quantity $(h\upsilon F(R_\infty))^2 = 0$

Table 3. Optical Bandgap energy and phase identification evidenced from XRD and Raman spectra for as-made and annealed samples deposited at different temperature using IPA

Glass Samples	Band gap, Eg(eV) ± 0.01	Cu foil samples	Bandgap, Eg(eV) ± 0.01	Phase composition (XRD and Raman)
G4(IPA30)	3.48	C4(IPA30)	3.47	ZnO
G5(IPA50)	3.37	C5(IPA50)	3.43	ZnO
G6(IPA65)	3.40	C6(IPA65)	3.45	ZnO
G4 Ann. 250 ℃	3.28	C4 Ann. 250 ℃	1.65 & 3.21	Cu_xO/ZnO
G5 Ann. 250 ℃	3.21	C5 Ann. 250 ℃	1.65 & 2.98	Cu_xO/ZnO
G6 Ann. 250 ℃	3.15	C6 Ann. 250 ℃	2.00 & 3.00	Cu_xO/ZnO

*Crystallite sizes of the samples grown on SLG substrate are shown in Table 2

From Table 3, it is clear that the E_g values are in the range of 3.37-3.47 eV for as-made samples and 2.98-3.28 eV those for post-annealing samples which could be attributed to the ZnO. However, post-annealing treatment in case of Cu foil samples exhibited additional Eg in the range of 1.65 – 2.00 eV(see dotted line in Figure 6b) which could be attributed to the Cu_xO phase[50]. Notice that samples deposited on SLG exhibited a reduction in bandgap with increasing IPA temperatures due to improve crystallinity of the ZnO and corroborates the calculated crystallite sizes given in Table 2.

Preprints (www.preprints.org) | NOT PEER-REVIEWED | Posted: 26 July 2020 doi:10.20944/preprints202007.0626.v1

However, post-annealing treatment induced a significant reduction of Eg from roughly 3.4 eV to 3.2 eV is due to the improvement of crystallinity [5] with decline of lattice strain (see Table 2). These observations imply that post-annealing treatment at 250 ℃ affected deposited films largely compared to IPA temperatures. It is worth noting that samples grown on Cu foil indicating the possibility of Cu_xO/ZnO junction formation by post-annealing (see Table 3). As a proof-of-concept, I-V characteristics curve of a preliminarily fabricated heterojunction by SILAR method with FTO/Cu_xO/ZnO/Al structure is shown in Figure 7, where the diode-like I-V curve confirms that Cu_xO/ZnO is successfully formed. However, further experimental investigations are in progress to assess photovoltaic performance of SILAR grown Cu_xO/ZnO junctions.

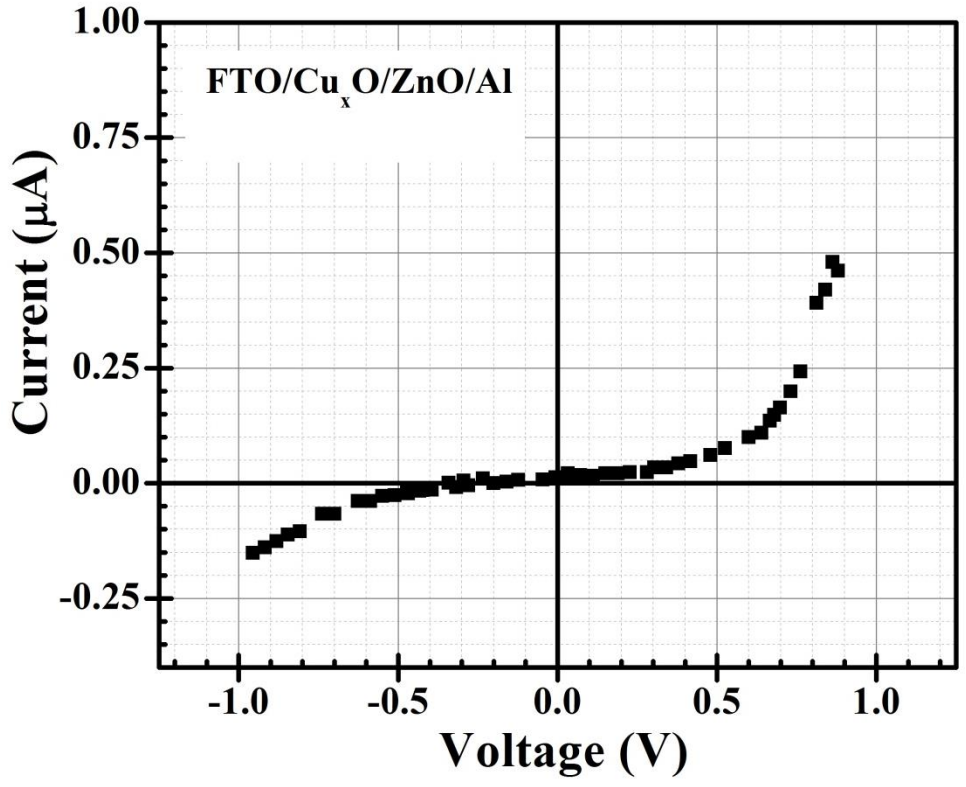

Figure 7. I-V characteristic curve of a SILAR grown heterojunction showing diode-like behaviour confirming the successful formation of Cu_xO/ZnO junction.

 doi:10.20944/preprints202007.0626.v1

4. Conclusion

ZnO thin films have been synthesized on both SLG and Cu foil and the effect of substrate, sonication process, and post-annealing on the properties of the deposited films were systematically investigated. XRD analysis revealed the growth of highly crystalline c-axis oriented ZnO thin films deposited on SLG with (002) preferred orientation while (101) preferential growth on Cu foil. XRD and Raman spectroscopy confirmed all of the post-annealing samples produce Cu_xO/ZnO heterojunctions irrespective to the growth temperature using IPA and sonication process. Samples excluding sonication steps exhibited compact and uniformly distributed grain surface morphologies in the presence of IPA at 50 and 65 ℃ observed from SEM micrographs. The estimated Eg values were 3.47-3.37 eV for as-made samples and bandgaps were found to be decreased significantly with increasing annealing temperature due to crystallinity improvement of the ZnO thin films. The sample grown at 50 ℃ revealed the best quality film grown in this work with the Eg value of 3.37 eV. This studies proposed that for highly c-axis oriented ZnO thin films, it may be better to deposit the films on SLG in presence of IPA as a dispersing agent. We hope that this study will open up a new approach for growing ZnO thin film with less processing steps as well as solution processable Cu-oxide/ZnO heterojunctions for diverse applications.

Author Contributions: B.C. Ghos performed the sample synthesis, data analysis and wrote the manuscript. N.I. Tanvir helped with the experimental methodology and characterization setups. M.A Majed Patwary and M.A. Rahman contributed to the conceptualization, and supervision. S. Majumder and M.A. Hossain contributed to the formal data analyses and scientific discussion of the

results. S.F.U. Farhad conceived the project idea, conceptualization, and led the overall research works. All authors contributed to the writing, reviewing and editing of the final manuscript.

Acknowledgments: S.F.U. Farhad and N.I. Tanvir acknowledge the experimental support of the Energy Conversion and Storage Research Section, Industrial Physics Division, BCSIR Laboratories, Dhaka 1205, under the scope of R&D project#100-FY2017-2020. M.A.M. Patwary acknowledges the characterization support of Department of Electrical and Electronic Engineering, Saga University, Japan. All other authors gratefully acknowledge the logistic support of Physical Chemistry Research Laboratory, Department of Chemistry, Comilla University, Cumilla 3506, Bangladesh.

Conflicts of Interest: The authors declare no conflicts of interest.

References:

1. Akhtar, M.S.; Riaz, S.; Noor, R.; Naseem, S. Optical and Structural Properties of ZnO Thin Films for Solar Cell Applications. *Adv. Sci. Letters* **2013,** *19(3)*, 834-841. DOI: 10.1166/asl.2013.4822
2. Muchuweni, E.; Sathiaraj, T.S.; Nyakotyo, H. Physical properties of gallium and aluminium co-doped zinc oxide thin films deposited at different radio frequency magnetron sputtering power. *Ceram. Int.* **2016**, *42*, 17706–17710. DOI: http://dx.doi.org/10.1016/j.ceramint.2016.08.091
3. Hsin-Chun, L.; Jia-Chiuan, J.; Chun-Lung, C. Influence of RF magnetron sputtering conditions on the properties of transparent conductive gallium-doped magnesium zinc oxide thin films.

Surface & Coatings Tech. **2013**, *231*, 539–542. DOI: http://dx.doi.org/10.1016/j.surfcoat.2012.10.029

4. Ashfold, M.N.R.; Doherty, R.P.; Ndifor-Angwafor, N.G.; Riley, D.J.; Sun, Y. The kinetics of the hydrothermal growth of ZnO nanostructures. *Thin Solid Films* **2007,** *515(24)*, 8679-8683. DOI:10.1016/j.tsf.2007.03.122

5. Shei, S.C.; Lee, P.Y. Influence of rinsing temperature on properties of ZnO thin films prepared by SILAR method with propylene glycol. *J. Alloys Compd.* **2013**, *546*, 165–170. DOI: http://dx.doi.org/10.1016/j.jallcom.2012.07.149

6. Joshi, K.; Rawat, M.; Gautam, S.K.; Singh, R.; Ramola, R.; Mahajan, A. Band gap widening and narrowing in Cu-doped ZnO thin films. *J. Alloy. Compd.* **2016**, *680*, 252–258. DOI: 10.1016/j.jallcom.2016.04.093

7. Rong, P.; Ren, S.; Yu, Q. Fabrications and Applications of ZnO Nanomaterials in Flexible Functional Devices-A Review. *Crit. Rev. Anal. Chem.* **2018**, *49*, 336–349. DOI: 10.1080/10408347.2018.1531691

8. Aoun, Y.; Benhaoua, B.; Benramache, S.; Gasmi, B. Effect of deposition rate on the structural, optical and electrical properties of Zinc oxide (ZnO) thin films prepared by spray pyrolysis technique. *Optik*. **2015**, *126*, 2481–2484. DOI: https://doi.org/10.1016/j.ijleo.2015.06.025

9. Gil, B.; Kavokin, A.V. Giant exciton-light coupling in ZnO quantum dots. *Appl. Phys. Lett.* **2002**, *81*, 748–750. DOI: 10.1063/1.1494864

10. Bretagnon, T.; Lefebvre, P.; Valvin, P.; Gil, B.; Morhain, C.; Tang, X. Time resolved photoluminescence study of ZnO/(Zn, Mg)O quantum wells. *J. Cryst. Growth* **2006**, *287*, 12–15. DOI: https://doi.org/10.1016/j.jcrysgro.2005.10.034

11. Xiong, C.; Yao, R.H.; Wan, W.J.; Xu, J.X. Fabrication and electrical characterization of ZnO rod arrays/CuSCN heterojunctions. *Optik.* **2014**, *125*, 785–788. DOI: https://doi.org/10.1016/j.ijleo.2013.07.080

12. Hassan, M.A.M.; Saleh, A.F.; Mezher, S.J. Energy band diagram of In:ZnO/p-Si structures deposited using chemical spray pyrolysis technique. *Appl. Nanosci*. **2014**, *4*, 695–701. DOI: 10.1007/s13204-013-0246-5

13. Manoharan, C.; Pavithra, G.; Bououdina, M.; Dhanapandian, S.; Dhamodharan, P. Characterization and study of antibacterial activity of spray pyrolysed ZnO: Al thin films. *Appl. Nanosci.* **2016**, *6*, 815–825. DOI: 10.1007/s13204-015-0493-8

14. Balaji, G.; Sivakami, R.; Sridharan, M.; Jeyadheepan, K. Preparation and characterization of refractory ZnO buffer layers for thin film solar cell applications. *Mater. Today Proc.* **2016**, *3*, 1730–1736. DOI: https://doi.org/10.1016/j.matpr.2016.04.067

15. Aoun, Y.; Benhaoua, B.; Benramache, S.; Gasmi, B. Effect of annealing temperature on structural, optical and electrical properties of zinc oxide (ZnO) thin films deposited by spray pyrolysis technique. *Optik.* **2015**, *126*, 5407–5411. DOI: https://doi.org/10.1016/j.ijleo.2015.08.267

16. Islam, M.R.; Podder, J.; Farhad, S.F.U.; Saha, D.K. Effect of Annealing on the Structural and Optical Properties of Nano Fiber ZnO Films Deposited by Spray Pyrolysis. *Sensors & Transducers.* **2011**, *134(11)*, 170-176.

17. Dhanakodi, K.; Thirunavukkarasu, P.; Mariappan, R.; Rajamanickam, A.T. Effect of substrate temperature on the nebulizer sprayed zinc oxide thin films. *Optik.* **2016**, *127*, 2516–2520. DOI:

https://doi.org/10.1016/j.ijleo.2015.10.143

18. Kenanakis, G.; Katsarakis, N.; Koudoumas, E. Influence of precursor type, deposition time and doping concentration on the morphological, electrical and optical properties of ZnO and ZnO: Al thin films grown by ultrasonic spray pyrolysis. *Thin Solid Films.* **2014**, *555*, 62–67. DOI: https://doi.org/10.1016/j.tsf.2013.10.015

19. Zhang. Z.; Liao, Q.; Yu, Y.; Wang, X.; Zhang, Y. Enhanced photoresponse of ZnO nanorods-based self-powered photodetector by piezotronic interface engineering, *Nano Energy.* **2014**, *9*, 237-244. DOI: https://doi.org/10.1016/j.nanoen.2014.07.019

20. Roy, S.; Banerjee, N.; Sarkar, C. K.; Bhattacharyya, P. Development of an Ethanol Sensor Based on CBD Grown ZnO Nanorods. *Solid-State Electron.* **2013,** *87*, 43-50. DOI: https://doi.org/10.1016/j.sse.2013.05.003

21. Singh, O.; Kohli, N.; Singh, R.C. Precursor Controlled Morphology of Zinc Oxide and its Sensing Behavior. *Sens. Actuators B.* **2013,** *178*, 149-154. DOI: https://doi.org/10.1016/j.snb.2012.12.053

22. Schmidt-Mende, L.; MacManus-Driscoll, J.L. ZnO–nanostructures, defects and devices. *Materials Today*. **2007**, *10(5)*, 40-48. DOI: https://doi.org/10.1016/S1369-7021(07)70078-0

23. Kadota, M. Surface Acoustic Wave Characteristics of a ZnO/Quartz Substrate Structure Having a Large Electromechanical Coupling Factor and a Small Temperature Coefficient. *Jpn. J. Appl. Phys.* **1997**, *36*, 3076-3080. DOI: https://doi.org/10.1143/JJAP.36.3076

24. Ennaceri, H.; Erfurt, D.; Wang, L.; Köhler, T.; Taleb, A.; Khaldoun, A.; El Kenz, A.; Benyoussef, A.; Ennaoui, A.; Ahmed, D.E. Deposition of multifunctional TiO_2 and ZnO top-protective

coatings for CSP application. *Surf. Coatings Technol.* **2016**, *298*, 103–113. DOI: https://doi.org/10.1016/j.surfcoat.2016.04.048

25. Wang, Z.L.; Song, J. Piezoelectric Nanogenerators Based on Zinc Oxide Nanowire Arrays. *Science.* **2006**, *312*, 242-246. DOI: 10.1126/science.1124005

26. Lee, P.Y.; Chang, S.P.; Chang, J.F.; Hsu, E.N.; Chang, S.J. Highly Transparent Nanostructured Zinc Oxide Photodetector Prepared by Successive Ionic Layer Adsorption and Reaction. *Int. J. Electrochem. Sci.* **2013**, *8*, 6425-6432.

27. Gao, X.; Xiaomin, L.; Weidong, Y. Preparation and characterization of highly oriented ZnO film by ultrasonic assisted SILAR method. *J. Wuhan Uni. Tech. Mater. Sci. Ed*. **2005**, *20*, 23-26. DOI: https://doi.org/10.1007/BF02835019

28. Ajuba, A.E.; Ezugwu, S.C.; Ezekoye, B.A.; Ezema, F.I.; Asogwa, P.U. Influence of pH on the structural, optical and solid state properties of chemical bath deposited ZnO thin films. *J. Optoelec. Biomed. Mater.* **2010,** *2(2)*, 73-78.

29. Villanueva, Y.Y.; Liu, D.R.; Cheng, P.T. Pulsed laser deposition of zinc oxide. *Thin Solid Films* **2006**, *501*, 366-369. DOI: https://doi.org/10.1016/j.tsf.2005.07.152

30. Cruz, M.R.A.; Ceballos-Sanchez, O.; Luevano-Hipolito, E.; Torres-Martı´nez, L.M. ZnO thin films deposited by RF magnetron sputtering: Effects of the annealing and atmosphere conditions on the photocatalytic hydrogen production. *Int. J. Hydro. Energ.* **2018**, *43(22)*, 10301-10310. DOI: https://doi.org/10.1016/j.ijhydene.2018.04.054

31. Ye, J.; Gu, S.; Zhu, S.; Chen, T.; Hu, L.; Qin, F.; Zhang, R.; Shi, Y.; Zheng, Y. The growth and annealing of single crystalline ZnO films by low-pressure MOCVD. *J. Cryst. Growth* **2002**, *243*,

151-156. DOI: https://doi.org/10.1016/S0022-0248(02)01474-4

32. Islam, M.R.; Rahman, M.; Farhad, S.F.U.; Podder, J. Structural,optical and photocatalysis properties of sol-gel deposited Al-doped ZnO thin films. *Surfaces and Interfaces.* **2019**, *16*, 120-126. DOI: https://doi.org/10.1016/j.surfin.2019.05.007

33. Baruah, S.; Dutta, J. Effect of seeded substrates on hydrothermally grown ZnO nanorods. *J. Sol-Gel Sci. Tech.* **2009**, *50(3)*, 456-464. DOI: https://doi.org/10.1007/s10971-009-1917-2

34. Kato, H.; Sano, M.; Miyamoto, K.; Yao, T. High quality ZnO epilayers grown on Zn-face ZnO substrates by plasma-assisted molecular beam epitaxy. *J. Cryst. Growth* **2004**, *265*, 375-381. DOI: https://doi.org/10.1016/j.jcrysgro.2004.02.021

35. Farhad, S.F.U.; Tanvir, N.I.; Bashar, M.S.; Hossain, M.S.; Sultana, M.; Khatun, N.; Facile synthesis of oriented zinc oxide seed layer for the hydrothermal growth of zinc oxide nanorods. *Bangladesh J. Sci. Ind. Res.* **2018**, *53(4)*, 233-244. DOI: 10.3329/bjsir.v53i4.39186

36. Farhad, S.F.U.; Tanvir, N.I.; Bashar, M.S.; Sultana, M. Synthesis and characterization of c-axis oriented Zinc Oxide thin films and its use for the subsequent hydrothermal growth of Zinc Oxide nanorods. *MRS Advances*. **2019**, *4(16)*, 921-928. DOI: https://doi.org/10.1557/adv.2019.65

37. Zhenghua, S.; Kaiwen, S.; Zili, H.; Fangyang, L.; Yanqing, L.; Jie, L.; Yexiang L. Fabrication of ternary Cu–Sn–S sulfides by a modified successive ionic layer adsorption and reaction (SILAR) method. *J. Mater. Chem.* **2012**, *22*, 16346–16352. DOI: https://doi.org/10.1039/C2JM31669B

38. Haridas, D.D.; Surendra, K.S.; Ninad, B.V.; Lohar, G.M.; Vijay, J.F. Synthesis and characterization of ZnO thin film by low cost modified SILAR technique. *AIMS Materials Science.* **2016**, *3(2)*, 349-356. DOI: DOI: 10.3934/matersci.2016.2.349

39. Raidou, E.A.; Benmalek, F.; Sall, T.; Aggour, M.; Qachaou, A.; Laanab, L.; Fahoume, M. Characterization of ZnO Thin Films Grown by SILAR Method. *Open Access Library Journal.* **2014**, *01(03)*, 1-9. DOI: 10.4236/oalib.1100588

40. Offiah, S.U.; Agbo, S.N.; Sutta, P.; Maaza, M.; Ugwuoke, P.E.; Osuji, R.U.; Ezema, F.I. *Journal of Solid State Electrochemistry*. **2017**, *21*, 2621–2628. DOI: https://doi.org/10.1007/s10008-017-3514-6

41. Farhad, S.F.U.; Hossain, M.A.; Tanvir, N.I.; Akter, R.; Patwary, M.A.M.; Shahjaha, M.; Rahman, M.A. Structural, optical, electrical, and photoelectrochemical properties of cuprous oxide thin films grown by modified SILAR method. *J. Mater. Sci. Semicon. Process.* **2019**, *95*, 68-75. DOI: https://doi.org/10.1016/j.mssp.2019.02.014

42. Mageshwari, K.; Sathyamoorthy, R. Physical properties of nanocrystalline CuO thin films prepared by the SILAR method. *Mater. Sci. Semicond. Process.* **2013**, *16(2)*, 337–343. DOI: https://doi.org/10.1016/j.mssp.2012.09.016

43. Patil, A.S.; Lohar, G.M.; Fulari, V.J. Structural, morphological, optical and photo-electrochemical cell properties of copper oxide using modified SILAR method. *J. Mater. Sci. Mater. Electron.* **2016**, *27(9)*, 9550–9557. DOI: https://doi.org/10.1007/s10854-016-5007-2

44. Beaini, S.S.; Kronawitter, C.X.; Carey V.P.; Mao, S.S. ZnO deposition on metal substrates: Relating fabrication, morphology, and wettability. *J. App. Phy.* **2013**, *113*, 184905-184914. DOI: https://doi.org/10.1063/1.4803553

45. Raidou, A.; Lharch, M.; Nouneh, K.; Aggour, M.; Qachaou, M.; Laanab, L.; Fahoume, M. Effect of substrate on ZnO thin flms grown by SILAR method. *Proceedings of 2014 International*

Renewable and Sustainable Energy Conference, IRSEC 2014, Ouarzazate, Morocco, 17-19 October **2014**. DOI: 10.1109/IRSEC.2014.7059829

46. Shei, S.C.; Lee, P.Y.; Chang, S.J. Effect of temperature on the deposition of ZnO thin films by successive ionic layer adsorption and reaction. *App. Surf. Sci.* **2012**, *258*, 8109-8116. DOI: http://dx.doi.org/10.1016/j.apsusc.2012.05.004

47. Shei, S.C.; Chang, S.J.; Lee, P.Y. Rinsing Effects on Successive Ionic Layer Adsorption and Reaction Method for Deposition of ZnO Thin Films. *J. Electrochem. Soc.* **2011**, *158(3)*, H208-H213. DOI: 10.1149/1.3528306

48. Farhad, S.F.U.; Majumder, S.; Hossain, M.A.; Tanvir, N.I.; Akter, R.; Patwary, M.A.M. Effect of Solution pH and Post-annealing temperatures on the Optical Bandgap of the Copper Oxide Thin Films Grown by modified SILAR Method. *MRS Advances* **2019**, *4(16)*, 937-944. DOI: 10.1557/adv.2019.139

49. Chowdhury, R.I.; Hossen, M.A.; Mustafa, G.; Hussain, S.; Rahman, S.N.; Farhad, S.F.U.; Murata, K.; Tambo, T.; Islam, A.B.M.O. Characterization of Chemically-deposited Cadmium Sulfide Thin Films. *Int. J. Modern Phys. B.* **2010**, *24*, 5901-5911. DOI: 10.1142/S0217979210055147

50. Farhad, S.F.U.; Webster, R.F.; Cherns, D. Electron Microscopy and Diffraction studies of Pulsed Laser deposited Cuprous oxide thin films grown at low substrate temperature. *Materialia.* **2018**, *3*, 230-238. DOI: https://doi.org/10.1016/j.mtla.2018.08.032

51. Singh, S.; Srinivasa, R.S.; Major, S.S. Effect of substrate temperature on the structure and optical properties of ZnO thin films deposited by reactive rf magnetron sputtering. *Thin Solid Films* **2007**, *515(24)*, 8718-8722. DOI:https://doi.org/10.1016/j.tsf.2007.03.168

52. Patwary, M.A.M.; Saito, K.; Guo,Q.; Tanaka,T. Influence of oxygen flow rate and substrate positions on properties of Cu-oxide thin films fabricated by radio frequency magnetron sputtering using pure Cu target. *Thin Solid Films*. **2019**, *675*, 59–65. DOI: https://doi.org/10.1016/j.tsf.2019.02.026

53. Koyano, M.; QuocBao, Q.; ThanhBinh, L.T.; HongHa, L.; NgocLong, N.; Katayama, S.I. Photoluminescence and Raman Spectra of ZnO Thin Films by Charged Liquid Cluster Beam Technique. *Phys. Stat. Sol.* **2002**, *193*, 125–131. DOI: **https://doi.org/10.1002/1521-396X(200209)193:1<125::AID-PSSA125>3.0.CO;2-X**

54. Yahia, S.B.; Znaidi, L.; Kanaev, A.; Petitet, J. P. Raman study of oriented ZnO thin films deposited by sol–gel method. *Spectrochimica Acta Part A* **2008**, *71*, 1234–1238. DOI: 10.1016/j.saa.2008.03.032

55. Farhad, S.F.U.; Cherns, D.; Smith, J.A.; Fox, N.A.; Fermín, D.J. Pulsed laser deposition of single phase n- and p-type Cu_2O thin films with low resistivity. *Materials and Design*. **2020**, *193*, 108848-108855. DOI: https://doi.org/10.1016/j.matdes.2020.108848

56. Patwary, M.A.M.; Ho, C.Y.; Saito, K.; Guo, Q.; Yu, K.M.; Walukiewicz, W.; Tanaka,T. Effect of oxygen flow rate on properties of Cu_4O_3 thin films fabricated by radio frequency magnetron sputtering. *J. Appl. Phys.* **2020**, *127*, 085302. DOI: https://doi.org/10.1063/1.5144205

57. Pandey, P.; Parra, M.R.; Haque, F.Z. Effects of annealing temperature optimization on the efficiency of ZnO nanoparticles photoanode based dye sensitized solar cells. *J Mater Sci: Matter Electron*. **2017**, *28*, 1537-1545. DOI: 10.1007/s10854-016-5693-9

58. Khan, A. Raman Spectroscopic Study of the ZnO Nanostructures. *J. Pak. Mater. Soc*. **2010**, *4(1)*, 5-9.

59. Li, H.; Ban, L.; Niu, Z.; Huang, X.; Meng, P.; Han, X.; Zhang. Y.; Zhang, H.; Zhao, Y. Application of Cu_xO-Fe_yO_z Nanocatalysts in Ethynylation of Formaldehyde. *Nanomaterials*. **2019**, *9*(9), 1301-1315. DOI: https://doi.org/10.3390/nano9091301

60. Mauricio Muñoz-Muñoz, Y.; Guevara-Carrion, G.; Jadran, V. Molecular Insight into the Liquid Propan-2-ol + Water Mixture. *J. Phys. Chem. B* **2018**, *122(37)*, 8718–8729. DOI: https://doi.org/10.1021/acs.jpcb.8b05610

61. Crupi, V.; Majolino, D.; Migliardo, P.; Venuti, V. Inter- and intramolecular hydrogen bond in liquid polymers: a Fourier transform infrared response. *Molecular Physics*, **2000**, *98*, 1589-1594. DOI: https://dx.doi.org/10.1080/00268970009483364

62. Daira, R.; Kabir, A.; Boudjema, B.; Sedrati, C. Structural and optical transmittance analysis of CuO thin films deposited by the spray pyrolysis method. *Solid Sate Sci*. **2020**, *104*, 106254-106257. DOI: https://doi.org/10.1016/j.solidstatesciences.2020.106254